Biochimica et Biophysica Acta 1850 (2015) 972–982

Contents lists available at ScienceDirect

Biochimica et Biophysica Acta

journal homepage: www.elsevier.com/locate/bbagen

Extension of the free energy workflow FEW towards implicit solvent/implicit membrane MM–PBSA calculations ☆

Nadine Homeyer, Holger Gohlke *

Mathematisch-Naturwissenschaftliche Fakultät, Institut für Pharmazeutische und Medizinische Chemie, Heinrich-Heine-Universität Düsseldorf, Germany

ARTICLE INFO

Article history:
Received 24 August 2014
Received in revised form 13 October 2014
Accepted 14 October 2014
Available online 23 October 2014

Keywords:
AMBER
Molecular dynamics simulations
Ion channel
Membrane protein
Drug design

ABSTRACT

Background: The number of high-resolution structures of pharmacologically relevant membrane proteins has been strongly increasing. This makes computing relative affinities of chemically similar compounds binding to a membrane protein possible in order to guide decision making in drug design. However, the preparation step of such calculations is time-consuming and complex.
Methods: We extended the free energy workflow tool FEW, available in AMBER, towards facilitating the setup of molecular dynamics simulations with explicit membrane, and the setup and execution of effective binding energy calculations according to a 1-trajectory implicit solvent/implicit membrane MM-PBSA approach for multiple ligands binding to the same membrane protein.
Results: We validated the implemented protocol initially on two model systems, a sodium ion in the presence of an implicit membrane slab and a proton traversing the M2 proton-channel of the influenza A virus. For the latter, we found a good agreement for several important events along the proton pathway with those obtained in a recent computational study. Finally, we performed a case study on effective binding energy calculations for a set of inhibitors binding to the M2 proton-channel.
Conclusions: From the case study, we estimate a considerable speed up in the setup and analysis times for implicit solvent/implicit membrane MM-PBSA calculations by the extended version of FEW compared to a manual preparation.
General significance: Together with the overall runtime and the analysis results, this suggests that such type of calculations can be valuable in later stages of drug design projects on membrane proteins. This article is part of a Special Issue entitled Recent developments of molecular dynamics.

1. Introduction

Membrane proteins constitute a large fraction of the human proteome and participate in pivotal cellular processes. It was estimated that 27% of the human proteins are α-helical transmembrane proteins [1]. Because of their central role in a vast variety of important physiological processes, the disfunction of membrane proteins can result in severe diseases [2]. Membrane proteins have thus evolved as primary drug targets, providing approximately 60% of the targets of approved drugs [3]. Predicting the binding affinity of potential ligands for membrane proteins is highly beneficial in drug design. One obstacle in the past, the lack of high-resolution structural information of membrane proteins, which is desirable for such predictions, is currently being overcome by large efforts for solving three-dimensional structures of membrane proteins [4]. This has already led to a plethora of new structures for, e.g., G-protein coupled receptors [5] and ion channels [6,7]. Another obstacle results from the fact that setting up such computations usually requires many separate, but repetitive, steps, which becomes tedious for even medium-sized compound sets. Here, we address this second obstacle by extending our *W*orkflow tool for *F*ree *E*nergy calculations of ligand binding, FEW [8], towards MM-PBSA calculations in an implicit solvent/implicit membrane environment.

Several approaches for computing the free energy of binding of ligands to a biomolecular target have been developed [9,10]. At the lower end with respect to computational demand are docking/scoring function-based approaches that allow a fast but only approximate estimation of binding affinities [10–12]. At the other end are computationally expensive, rigorous, pathway-based free energy calculations such as free energy perturbation or thermodynamic integration that allow, in ideal cases, predictions within ~1 kcal/mol [13,14]. In between these two extremes, there are the so-called end-point approaches that consider only the initial (unbound) and final (bound) states of the binding process [10,15–18]. The continuum solvent approaches, in which the end-states are described using an implicit model for the solvent, belong to this category. Among these, the molecular mechanics Poisson–

☆ This article is part of a Special Issue entitled Recent developments of molecular dynamics.

* Corresponding author at: Universitätsstr. 1, 40225 Düsseldorf, Germany. Tel.: +49 211 81 13662; fax: +49 211 81 13847.
E-mail address: gohlke@uni-duesseldorf.de (H. Gohlke).

http://dx.doi.org/10.1016/j.bbagen.2014.10.013
0304-4165/

Boltzmann surface area (MM-PBSA) method [17] is likely the most widely used one. This method has proven capable to accurately predict the relative binding affinity of similar ligand compounds [19–22] while requiring only a moderate computational effort.

In the last years, a number of tools for semi-automated binding free energy calculations have been developed [8,23–31]. Among these are also tools for semi-automated MM-PBSA calculations such as the BEAR workflow [31], PyMOL plugins intended as a drug design platform [24], and our workflow tool FEW [8]. However, none of these tools has been specifically developed for binding free energy calculations on membrane protein–ligand systems.

In conventional MM-PBSA calculations, the polar part of the solvation free energy is computed by solving the Poisson–Boltzmann equation for the molecular system embedded in a continuum with a high dielectric constant, representing water. Such a setup is not appropriate for ligand binding to a membrane protein, however, because it does not account for the influence of the membrane on the protein–ligand interactions. This influence can be particularly large if the binding site is located close to the membrane lipids or within the transmembrane region of an integral membrane protein. Therefore, the membrane should be taken into account in the continuum solvent free energy calculations. For generating conformational ensembles of the membrane protein by molecular dynamics (MD) simulations this is done explicitly in order to account for the complex properties of the membrane. Retaining the explicit membrane representation also in the subsequent continuum solvent calculations would considerably increase the computational cost of the binding free energy calculations, not least because of the slow relaxation times observed within membranes [32], which would require long sampling times to generate appropriate thermodynamic ensembles to average over. One of the approaches to overcome this is to consider the membrane influence by an implicit membrane representation in the binding free energy calculations instead. Several implicit membrane models for continuum solvent calculations have been developed [33–35], and implicit solvent/implicit membrane calculations were successfully used to study peptide–membrane association thermodynamics and peptide–membrane interactions [33,35]. Nevertheless, implicit membrane models have not been used routinely so far in the context of free energy calculations of protein–ligand binding, although programs exist that provide the required functionality. These include the Poisson–Boltzmann solvers Delphi [36], PBSA [37], PBEQ [38,39] and the Adaptive Poisson–Boltzmann Solver (APBS) [40], all of which allow one to consider the membrane as a slab with a low dielectric constant embedded in a medium with the dielectric constant of water in Poisson-Boltzmann calculations. Tools that facilitate the setup of such calculations have recently become available [41–44]. Among these, the APBSmem [41] program is especially easy to use, because it allows to model and graphically inspect the membrane and to perform Poisson–Boltzmann calculations. That way, the setup for individual structures of the respective membrane protein can be directly tested. In our view, this makes APBSmem the ideal basis for a graphics-based setup of implicit solvent/implicit membrane Poisson–Boltzmann calculations.

In order to enable a fast setup and execution of free energy calculations for multiple ligands binding to the same membrane protein, we extended the functionality of FEW [8] towards facilitating implicit solvent/implicit membrane MM-PBSA calculations. In this extended FEW version, calculations of the polar part of the solvation free energy are prepared and conducted with APBS [40] allowing easy parameter selection with APBSmem [41]. The validity of the implemented calculation protocol is shown I) by solvation free energy calculations for a sodium ion in the presence of an implicit membrane slab, II) by the calculation of the profile of the polar interaction energy of a proton traversing the transmembrane domain of the M2 protein (M2TM) of the influenza A virus, and III) by effective binding energy calculations according to the implicit solvent/implicit membrane MM-PBSA approach implemented in FEW for a test set of ligands binding to M2TM.

2. Materials and methods

2.1. Computation of the solvation free energy of a sodium ion in the presence of an implicit membrane slab

A sodium ion with a radius of 1 Å and a charge of +1 was placed in 2 Å intervals from -30 Å to 30 Å along the z-axis. For each position of the sodium ion the polar part of the solvation free energy was calculated according to the following protocol:

Dielectric, charge, and ion-accessibility κ maps of the system were generated with APBS [40,45,46]. A grid of 80 Å × 80 Å × 80 Å, centered at the sodium ion, with 161 grid points in each direction was generated. A cubic B-spline charge discretization with default parameters was applied, and the dielectric coefficient as well as the ion-accessibility were defined according to the "mol" option using a sphere density of 10.0 points per Å^2 for the molecular surface definition. The bulk concentration of mobile ion species was set to 0 M. A dielectric constant of 80 was used for the solvent, and ε_{solute} was set to 1, 2, 4, and 5 in different calculations.

In the generated maps a membrane slab with $\varepsilon_{membrane} = 2$ was defined employing the draw_membrane2 [47] program. The membrane slab was created in the x–y plane of the coordinate system such that the sodium ion crosses the membrane in an orthogonal direction. A lower boundary of −19 Å and a thickness of 34 Å were defined for the membrane. This resulted in a planar slab reaching from −19 Å to +15 Å in z-axis direction.

For each position of the sodium ion the polar part of the solvation free energy at $T = 298.15$ K was computed with APBS [40,45,46] using the generated maps and employing the linearized Poisson–Boltzmann equation and Dirichlet boundary conditions. The polar part of the solvation free energy was obtained by substracting the charging free energy in vacuum, obtained from a calculation in a medium with a dielectric constant corresponding to ε_{solute}, from the charging free energy computed for the implicit solvent/implicit membrane state based on the generated maps.

The computed polar solvation free energies of the sodium ion were compared to the electrostatic transfer free energy that can be calculated by the Born equation (Eq. (1); in kcal mol^{-1}) [48] for a charge q located at the center of a sphere with radius a possessing a dielectric constant of ε_{solute} and being surrounded by a medium with $\varepsilon_{external}$

$$\Delta G^0 = \left(166\, q^2/a\right) \times \left(1/\varepsilon_{external} - 1/\varepsilon_{solute}\right) \quad (1)$$

with $a = 1$ Å and $q = +1$.

2.2. Computation of the polar interaction energy of a proton along the pore of the M2TM ion channel

Calculations were conducted using a crystal structure of the transmembrane part of the influenza A M2 proton-channel (M2TM, residues 22–46) (PDB ID: 3C9J) [49,50]. This structure was solved at pH 5.3 and can therefore be assumed to represent the proton-conducting, "open" state of the M2TM channel. The presence of the drug amantadine bound to the channel in the crystal structure is unlikely to considerably effect the conformation of the proton-conducting state, because only marginal differences were found in the N-terminal drug binding site region between this structure and a structure of the *apo* state solved at pH 7.3 (PDB ID: 3BKD) [50]. For the computations, the bound amantadine was removed, the present G34A mutation was reversed, and the amino acid Ser22 was deleted from all four chains of the tetrameric channel. The latter was necessary to avoid van der Waals clashes between atoms of Ser22 and the proton inserted later. As the region of the M2TM channel is part of a longer protein chain, acetyl- and *N*-methyl-amino blocking groups were attached to the terminal amino acids of the M2TM structure. Then, in total 61 structures were created

in which a proton with charge +1 and a radius of 1.4 Å was positioned in 1 Å intervals from 30 Å to −30 Å along the axis through the channel pore (z-axis). The His37 tetrad was modeled either in the (+2) or the (+3) state, corresponding to 2 or 3 charged histidines. In the (+2) state, two oppositely positioned histidines were positively charged. All neutral histidines were modeled in the Nε2-protonated state.

Electrostatic interaction energies ($E_{\text{ele, interaction } H^+ \text{ in channel}}$) between the proton in different positions along the pore axis and the M2TM channel were computed from Coulomb energies for the *apo* channel ($E_{\text{ele, M2TM}}$) and the channel in the presence of H^+ ($E_{\text{ele, M2TM}+H^+}$) by Eq. (2).

$$E_{\text{ele, interaction } H^+ \text{ in channel}} = E_{\text{ele, M2TM}+H^+} - E_{\text{ele, M2TM}} \quad (2)$$

Coulomb energies for the individual structures were computed by single-point molecular mechanics calculations with the mm_pbsa.pl script of AMBER [51,52] employing the ff10 force field [53,54] and using a dielectric constant equal to $\varepsilon_{\text{solute}}$ applied in the APBS calculations (see next paragraph).

The polar part of the solvation free energies were computed with APBS [40,45,46] using the same parameter settings described for the sodium ion above, except that now a bulk salt concentration of 0.15 M was applied to model physiological conditions. For the bulk ions radii of 2 Å and charges of +1 and −1 were used. The polar part of the solvation free energies were computed for *apo* M2TM ($G_{\text{PB, M2TM}}$) and M2TM with H^+ ($G_{\text{PB, M2TM}+H^+}$) in an implicit solvent/implicit membrane environment with $\varepsilon_{\text{membrane}} = 2$. Maps for an implicit membrane were prepared as for the sodium ion. However, a lower boundary of 14.7 Å and a membrane thickness of 29.4 Å were specified, which correspond to the region of the membrane for the 3C9J entry in the OPM database [55]. Furthermore, to ensure that the central pore of the channel was filled with implicit water with $\varepsilon_{\text{solvent}} = 80$, exclusion radii were provided to the draw_membrane2 [47] program: An upper exclusion radius of 11 Å and a lower exclusion radius of 15 Å were used (see Ref. [41] for a detailed explanation of the exclusion radius definition). In addition, the polar solvation energy of H^+ ($G_{\text{PB, } H^+}$) in implicit water ($\varepsilon_{\text{solvent}} = 80$) was computed using a grid of the same size and with the same spacing as for the implicit solvent/implicit membrane calculations. Finally, the change in the polar part of the solvation free energy of the proton in the presence of the channel was calculated according to Eq. (3).

$$G_{\text{PB, } H^+ \text{ in channel}} = G_{\text{PB, M2TM}+H^+} - G_{\text{PB, M2TM}} - G_{\text{PB, } H^+} \quad (3)$$

The calculations of the polar part of the solvation free energy were conducted with $\varepsilon_{\text{solute}} = 2$ and $\varepsilon_{\text{solute}} = 5$.

The total polar interaction energy of the proton in the channel ($E_{\text{total polar, } H^+ \text{ in channel}}$) was computed as the sum of the electrostatic interaction energy and the polar part of the solvation free energy (Eq. (4)).

$$E_{\text{total polar, } H^+ \text{ in channel}} = E_{\text{ele, interaction } H^+ \text{ in channel}} + G_{\text{PB, } H^+ \text{ in channel}} \quad (4)$$

2.3. Extension of the free energy workflow FEW

The FEW [8] program written in Perl was adapted and extended to enable the preparation of MD simulations with an explicit membrane. In addition, the program now allows setting up and executing effective binding energy calculations according to a 1-trajectory implicit solvent/implicit membrane MM-PBSA approach. For the execution of the effective energy calculations a stand-alone Perl program called *mmpbsa_FEWmem.pl* was written that handles the individual calculation steps conducted with the external programs mm_pbsa.pl [51,52], draw_membrane2 [47], APBS [40,45,46], and mm_pbsa_statistics.pl [51]. A detailed description of the implemented implicit solvent/implicit membrane free energy calculation procedure is given in the "Results and discussion" section.

2.4. Show case example for effective binding energy calculations by the implicit solvent/implicit membrane approach implemented in FEW

The implicit solvent/implicit membrane MM-PBSA approach was tested by computing effective binding energies for a data set of amantadine derivatives binding to the M2TM channel. Six ligands were selected from a set of small molecules for which binding affinities for M2TM had been experimentally determined by measuring the inhibition of the quenching of the fluorescence of Trp41 by protonation of His37 [56]. The selection was made such that the range of binding affinities spanned by the compounds was as large as possible, and only compounds were chosen for which the relative change in the configurational entropy upon binding could be expected to be negligible. With the latter criterion, we avoided that compounds with, e.g., a floppy ring system attached to the adamantane core were part of the data set. This is important because changes in the configurational entropy of the ligand and the M2TM channel upon complex formation are not explicitly calculated by normal mode [57,58] or quasiharmonic analysis [59] in the applied MM-PBSA procedure (entropic effects are only implicitly accounted for in the Poisson–Boltzmann calculations): The effective binding energy computed by the MM–PBSA approach in FEW considers only the changes in gas phase and solvation free energy upon binding. Hence, it is referred to as "effective binding energy" ($\Delta G_{\text{effective}}$) [8,58] to differentiate it from the binding free energy, in which changes in the configurational entropy are taken into account.

The complex structure of the M2TM channel with amantadine bound to the channel pore (PDB ID: 2KQT) [60] served as a model system to generate a starting structure for the molecular dynamics (MD) simulations of the M2TM-amantadine complex (see below). The structure was solved at pH 7.5. To model the conditions of the experimental binding affinity measurements conducted at pH 5 [56] two His37 residues in opposing positions were positively charged. Since it was found that the pK_a of His37 drops to approximately 5.4 in the presence of amantadine, it can be assumed that at least two out of the four histidines are charged at pH 5 [61]. All neutral histidines were modeled in the Nε2-protonated state because this state was reported to be more prominent by 3:1 than the Nδ1-protonated state [62], and this constellation of two doubly protonated and two Nε2-protonated histidines has successfully been used to model the configurations of His37 that have been observed for (+2) *apo* M2TM [63]. As it has been reported that water molecules are preferably located at certain positions inside the M2TM channel, water molecules were taken from the high resolution structure (PDB ID: 3LBW) [64] after superpositioning the backbone atoms of residues 25 to 46. All four chains of the M2TM tetramer were blocked by acetyl- and *N*-methyl-amino groups to account for the fact that each pore-forming protomer is part of a longer protein chain. The M2TM model system was then inserted into a 1,2-dimyristoyl-*sn*-glycero-3-phosphocholine (DMPC) bilayer extending at least 25 Å in x and y directions from M2TM using the "System builder" functionality of Desmond [26,27]. To model the experimentally used salt concentration, the system was solvated in a 0.10 M NaCl solution [56]. Positioning of ions inside the channel pore was prevented by ensuring that the distance between the channel as well as the membrane lipids and any ion was ≥6 Å using the "randomizeions" functionality of *ptraj* of AmberTools12 [65]. Topology and coordinate files of the generated M2TM-amantadine complex model system were prepared with *LEaP* [65].

Molecular dynamics (MD) simulations of the (+2) state M2TM-amantadine complex were conducted using the ff10 force field [53,54] for the protein, parameters from Joung and Cheatham [66,67] for the ions, the GAFFlipid parameters from Dickson et al. [68] for the DMPC lipids, and RESP charges [69] calculated with *Gaussian03* [70] and *antechamber* [65] as well as parameters from the general AMBER force field (GAFF) [71] for the ligand amantadine. All MD simulations were performed with the CPU versions of *sander* or *pmemd* of Amber12 [51]. After a thorough minimization of the system, it was heated to 303 K and equilibrated in a sequence of MD simulations. Production

simulations were carried out under NPTγ conditions (with $T = 303$ K and $\gamma = 10$ dyn cm^{-1}) for a total of 80 ns. A detailed description of the complete simulation protocol is provided in the Supporting information. The validity of this protocol for DMPC lipid bilayer systems was tested and will be reported elsewhere (N. Homeyer & H. Gohlke, unpublished results).

Snapshots recorded in intervals of 20 ps were analyzed using *ptraj* [72] of AmberTools12 [65] and the *ptraj* extension routines of Hannes Loeffler [73]. Structures were visualized with pymol [74], and data were plotted with gnuplot [75] and Grace [76].

M2TM-ligand complexes for the effective binding energy calculations were generated based on the snapshot recorded after 80 ns of production MD simulation of the M2TM-amantadine complex system. Ligand structures were manually drawn with SYBYL-X [77] and optimized with moloc [78] using the MAB force field [79,80]. The prepared ligand structures were then superimposed onto the amantadine molecule of this snapshot using ROCS and the TanimotoCombo score [81,82]. Mol2 files of the ligands in the position obtained from the fit to the amantadine molecule were generated and used as ligand input structures for FEW. The M2TM structure from the snapshot served as input structure for the receptor. In addition, a PDB file with all lipids, ions, and water molecules from the snapshot was prepared and used as an input file of the membrane system for FEW.

Minimizations and MD simulations were prepared with FEW employing the new membrane setup functionality and using a protocol similar to the one used for the M2TM-amantadine simulation described above. Input structures of the M2TM-ligand complexes for the simulations were automatically prepared with FEW, removing all water molecules that were within a distance of 1.5 Å of the ligands to avoid clashes. Charges for the ligands were computed according to the RESP procedure [69] with *Gaussian09* [83] and *antechamber* [65]. Details of the simulation protocol are provided in the Supporting information. Production simulations of 5 ns length were generated, and snapshots of the systems were recorded in intervals of 20 ps along the trajectories. The MD simulations were run with the CPU versions of *sander* and *pmemd* of Amber12 [51] on a compute cluster employing 16 cores per system and were completed within ~2 days.

Effective binding energies for the ligands were computed by the 1-trajectory implicit solvent/implicit membrane MM-PBSA approach implemented in FEW. The calculations were conducted based on the 250 snapshots recorded during the MD simulations of the M2TM-ligand systems. For the implicit membrane slab a lower boundary of −19.95 Å and a thickness of 33.4 Å were specified. These values correspond to the average membrane position found in the last 30 ns of the MD simulation of the M2TM-amantadine complex based on electron density profiles (Fig. S1). Upper and lower exclusion radii of 12 Å and 15 Å were selected based on visual inspection using APBSmem [41]. MM-PBSA calculations were conducted with *mmpbsa_FEWmem.pl* with standard settings, using $\varepsilon_{membrane} = 2$ and $\varepsilon_{solute} = 1$ or 5, respectively. Solvation free energy computations with APBS [40,45,46] were carried out with the same grid definitions and parameter settings described for the sodium ion calculations above except that a bulk salt concentration of 0.15 M was employed.

The correlation between the computed binding free energies and experimental binding affinities was plotted and statistically analyzed with R [84].

3. Results and discussion

3.1. Profile of the polar part of the solvation free energy of a sodium ion in the presence of a membrane slab

For effective binding energy calculations of membrane protein–ligand systems by the MM-PBSA approach a protocol for computing the polar part of the solvation free energy in an implicit solvent/implicit membrane environment with the Adaptive Poisson–Boltzmann Solver (APBS) [40] was established (see "Materials and methods" section). In order to validate this protocol on a simple model system, the polar part of solvation free energies for a sodium ion with a radius of 1 Å placed in 2 Å intervals along the normal of an implicit membrane slab were computed (Fig. 1); for the solvent and the membrane $\varepsilon_{solvent} = 80$ and $\varepsilon_{membrane} = 2$ were used, respectively. Using $\varepsilon_{solute} = 1$, values computed that way for the sodium ion either placed at a large distance from the membrane (~±30 Å) or being centered in the membrane (~−2.0 Å) are in very good agreement (difference < 0.45 kcal mol^{-1}) with electrostatic transfer free energies calculated analytically by the Born equation (Eq. (1)) [48] using $\varepsilon_{external} = 80$ or $\varepsilon_{external} = 2$, respectively (horizontal gray lines in Fig. 1). Furthermore, consistent with expectations, the polar part of the solvation free energy decreases in the solvent region nearly inversely proportional with increasing ε_{solute}. In the center of the membrane, the polar part of the solvation free energy approaches zero when $\varepsilon_{solute} = 2$, and becomes positive for $\varepsilon_{solute} > \varepsilon_{membrane}$. Finally, to test whether the solvation free energy is correctly computed even if the membrane slab is not symmetrically arranged relative to the origin (which may occur in membrane protein–ligand systems if the membrane protein is used to define the origin; see below), the membrane slab was positioned asymmetrically along the z-axis. The asymmetrical arrangement is clearly reflected in the computed solvation free energies, which increase considerably at −18 Å and +14 Å where the ion enters the implicit membrane slab (vertical gray lines in Fig. 1). In summary, our protocol for computing the polar part of the solvation free energy in an implicit solvent/implicit membrane environment with APBS correctly reproduces absolute and relative values for a model system, even for an asymmetrically arranged implicit membrane slab.

3.2. Profile of the polar interaction energy of a proton passing through the M2TM channel

Next, we validated the protocol on a more complex system including a transmembrane protein. For this we computed the polar interaction energy (Eq. (4)) of a proton positioned in 1 Å intervals along the axis through the transmembrane domain of the M2 channel (M2TM) of the influenza A virus. Free energy profiles of a proton passing through differently charged states of this channel have recently been determined by Liang et al. using a computationally expensive, multi-scale simulation approach including quantum, classical, and reactive molecular dynamics methods (see Ref. [85] and Fig. 3 therein). Here, we tested whether the energy profiles can overall be reproduced by comparatively simple computations of the electrostatic interaction energy (Eq. (2)) plus the polar part of the solvation free energy (Eq. (3)).

We modeled the proton as a sphere with a +1 charge and a radius of water (1.4 Å) to reflect that the proton is solvated in aqueous solution. Note that the choice of the radius is somewhat ad hoc because H_3O^+, often used to represent the nature of a proton in water, has an effective ionic radius of 1.0 Å, i.e., smaller than the molecular radius of water [86], whereas in reality the proton is bound to several molecules of water, resulting in ionic species with larger effective radii. M2TM was represented by a single conformation taken from the crystal structure (PDB ID: 3C9J) [50], which is assumed to represent the proton-conducting, "open" state of the M2 channel [50,85,87]. Two charge states of M2TM were considered, the (+2) and the (+3) state, in which two or three of the four His37 residues are protonated and positively charged. These two charge states are considered the most relevant ones when proton conduction takes place if an additional (excess) proton is present [85,88,89].

Recently, Nielsen et al. reported that a solute dielectric constant in the range 2–5 is optimal to reproduce the electric field in protein systems by Poisson–Boltzmann calculations on fixed conformations [90]. Furthermore, the proton has to pass through a highly charged, narrow region of the channel where the applied implicit solvation model can be expected to underestimate the charge screening by (explicit)

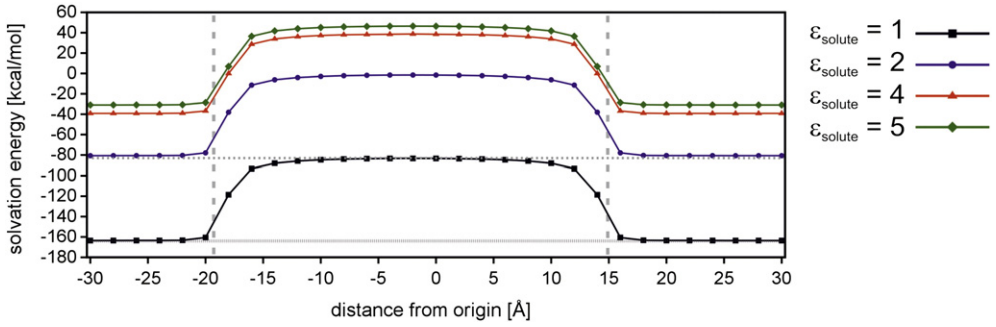

Fig. 1. Polar part of the solvation free energy of a sodium ion depending on its position relative to an implicit membrane slab. The solvation free energy was computed by the Poisson–Boltzmann approach applying $\varepsilon_{solvent} = 80$, $\varepsilon_{membrane} = 2$, and values in the range 1–5 for ε_{solute}, i.e., the dielectric constant of the sodium ion. The boundaries of the implicit membrane are indicated by long dashed, vertical gray lines. For $\varepsilon_{solute} = 1$ electrostatic transfer free energies computed by the Born equation (Eq. (1)) for a sodium ion in water ($\varepsilon_{external} = 80$) and in an environment with $\varepsilon_{external} = 2$ are marked by short dashed and dotted, horizonal gray lines, respectively.

solvent. This situation is reminiscent of effective binding energy computations by the MM-PBSA approach for systems with polar protein binding site-ligand interactions, where using a dielectric constant above unity for the solute has been found to be beneficial [20,91]. Taken together, this led us to compute the profiles of the polar interaction energy of the proton in M2TM applying $\varepsilon_{solute} = 2$ and $\varepsilon_{solute} = 5$.

The profiles of the polar interaction energy for the (+2) and (+3) charge states and $\varepsilon_{solute} = 5$ are shown in Fig. 2. Regarding several important events along the pathway of the proton through the pore, these profiles are remarkably similar to the free energy profiles found by Liang et al. [85]. First, we find a minimum in the polar interaction energy of −6.9 kcal mol^{-1} for the (+2) state (−5.9 kcal mol^{-1} for the (+3) state) when the proton reaches the interface between bulk water and the pore entrance flanked by Asp24 from the extracellular side (top side in Fig. 2) at a distance of ~16 Å from the origin. Liang et al. [85] find a similar minimum (~−2.5 kcal mol^{-1}) located at ~14 Å from the origin. The authors attributed its location close to Val27 to the anisotropic solvation structure of the hydrated proton, which, according to the authors, makes the proton somewhat amphiphilic in nature. In our case, in the absence of explicit water, we find a disfavorable contribution from the polar part of the solvation free energy as the proton approaches the narrow entrance of M2TM, which is overcompensated by a favorable Coulomb energy likely resulting from interactions between the proton and Asp24 (Fig. S2). Note that the M2TM structure used by Liang et al. [85] is shorter by two amino acids at the N-terminal end than ours, i.e. it lacks Ser23 and Asp24, which may explain the subtle difference in the location of the minima and the difference in the explanations as to the structural causes for the minima.

Second, the polar interaction energy steeply increases when the proton approaches Val27 and reaches a maximum of 14.8 kcal mol^{-1} for the (+2) state (16.6 kcal mol^{-1} for the (+3) state) in the region of Val27 (Fig. 2). The height of the maximum is comparable to the large free energy barrier observed by Liang et al. (~10 kcal mol^{-1}) between Val27 and His37 and confirms the important role of Val27 for the function of M2TM [87]. For the (+2) state, Liang et al. attributed this barrier in part to the ice-like character of water in the channel [85], which inhibits a proton transfer due to the slow water dynamics [85,92,93]. In

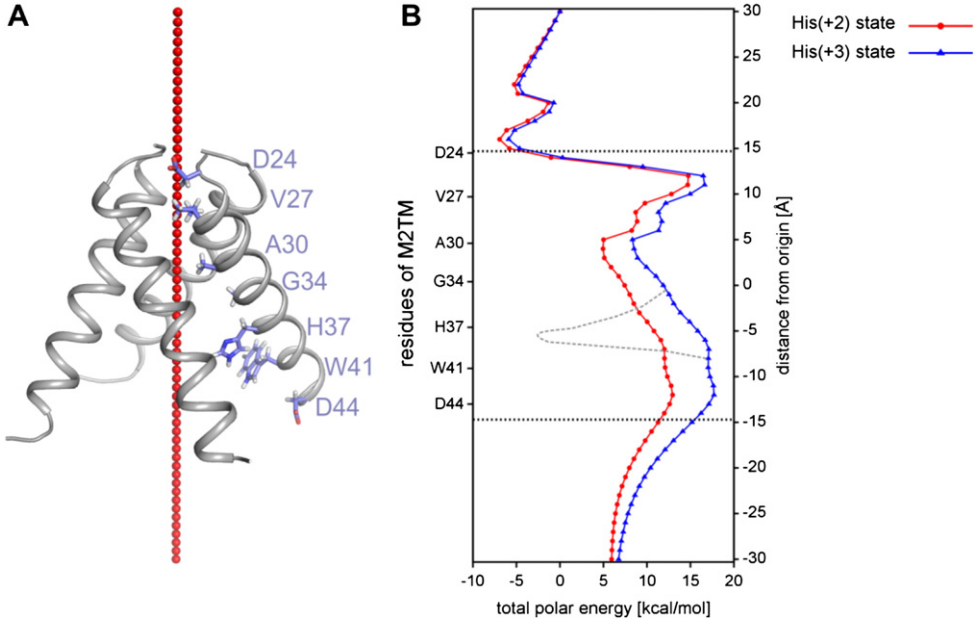

Fig. 2. Profile of the polar interaction energy of a proton moved in 1 Å steps along the axis of the pore of the M2TM channel in the (+2) or (+3) state, respectively. A: Ion positions relative to the channel visualized with Pymol [74]. The M2TM channel is shown in cartoon representation, amino acids of one protomer lining the pore are depicted as sticks, and the proton is represented as a red sphere. B: Total polar interaction energy (Eq. (4)) computed as the sum of the electrostatic energy (Eq. (2)) and the polar part of the solvation free energy (Eq. (3)) and normalized relative to the energy of the proton position most distant to the extracellular ("top") surface of the membrane at +30 Å. The polar part of the solvation free energies were computed with $\varepsilon_{solute} = 5$. The origin in the structure 3C9J is taken as the origin here [50]. The gray dotted line schematically depicts the deep minimum found by Liang et al. in the vicinity of the His37 tetrad.

our case, the maximum is mainly caused by the desolvation cost for transferring the proton from the solvent to the nonpolar channel interior (Fig. S2B) and the lack of a favorable Coulomb energy (Fig. S2A).

Third, considering a proton location beyond the His37 tetrad, we find another barrier in the polar interaction energy in the region of Trp41 (~12 Å from the origin) of 13.0 kcal mol^{-1} for M2TM in the (+2) state (17.7 kcal mol^{-1} in the (+3) state). Liang et al. [85] observed a similar barrier of ~10 kcal mol^{-1} (at ~11 Å from the origin for the (+2) state), which they attributed to the deprotonation of a histidine. Our barrier is caused by unfavorable Coulomb interactions of the proton in the region between His37 and Trp41 (Fig. S2A) that are not compensated by the polar part of the solvation free energy (Fig. S2B).

Regarding our profile and the free energy profile by Liang et al., there is one major difference around the His37 tetrad (~6 Å from the origin), however. In the work of Liang et al. the proton protonates histidine, which results in a free energy decrease by ~13 kcal mol^{-1} that culminates in a deep minimum (depicted as a gray dotted line in Fig. 2B). Obviously, using classical electrostatics, we cannot observe the histidine protonation and, hence, our profile of the polar interaction energy does not show a minimum there. Yet, we find it noteworthy to mention that estimates of the free energy of protonation of a solvated histidine obtained in two different ways (see Figs. S4 and S5) yield values between ~−20 kcal mol^{-1} and ~−10 kcal mol^{-1}. These values are in surprisingly good agreement with the free energy decrease observed by Liang et al. [85], although in our case the presence of charged histidines of the His37 tetrad and any effect due to charge delocalization is either not (Fig. S4) or only implicitly (Fig. S5) taken into account.

Finally, another difference arises when comparing the profiles for the (+2) and (+3) states. In this work and in the study by Liang et al. both profiles are similar in shape. However, in the study by Liang et al. the profile for the (+3) state shows lower barriers than that for the (+2) state, whereas in our case the barriers are higher. This is a result of the fact that in the study of Liang et al. the M2TM channel can adapt to the charge change and does so by widening, leading to a better solvation and, thus, a better screening of electrostatic repulsion and a larger water dynamics [85]. In our case of a fixed M2TM conformation, the additional charge in the (+3) state leads to an increased electrostatic repulsion around the His37 tetrad (Fig. S2A), which is not compensated by a more favorable polar part of the solvation free energy there (Fig. S2B).

In all, we performed our calculations of a proton transfer through the M2TM channel with no intention to condemn the highly sophisticated study of Liang et al. Rather, we intended to use their work to validate our protocol of computing polar interaction energies in an implicit solvent/implicit membrane environment and including a transmembrane protein. In that respect, it is encouraging to see the at least qualitative, if not semi-quantitative, agreement for several important events along the pathway of the proton through the pore. At the same time, the above computations also reveal limitations of the chosen approach. Along these lines, one not yet mentioned is the dependence of the results on the choice of ε_{solute}: Although the shape of the profiles is very similar for $\varepsilon_{solute} = 2$ or 5, the magnitudes of the minima and maxima increase considerably for $\varepsilon_{solute} = 2$ (Fig. S3) compared to $\varepsilon_{solute} = 5$ (Fig. 2B).

3.3. Extension of FEW towards implicit solvent/implicit membrane MM-PBSA calculations

The workflow tool FEW was extended with the aim to provide the functionality for an easy setup and execution of effective binding energy calculations for membrane protein–ligand systems by an ensemble-based implicit solvent/implicit membrane MM-PBSA approach. The original FEW already comprised a module for conventional MM-PBSA calculations (WAMM, [8]). The module can be invoked by a command-line call of the main FEW routine together with the name of the procedure ("MMPBSA") and a text file with parameter specifications ("command file") (Fig. 3). FEW requires as input a PDB structure of the protein and structures of the ligands in Mol2 format. Initially, the validity of the provided files and specified parameters is checked. The MM-PBSA workflow then starts with the preparation of protein–ligand systems and input files for MD simulations.

In the extended version, FEW now allows setting up MD simulations for membrane protein–ligand complexes embedded in an explicit membrane bilayer. For the preparation of such simulations the user needs to provide a PDB file containing information about the lipids, ions, and water molecules, in addition to the input files of the protein and the ligand structures. Such a PDB file can be prepared, e.g., with the CHARMM-GUI Membrane Builder [94–96], the ProBLM server [43], or the "System Builder" of Desmond [26,27]. One needs to take care in that process that the atom and residue names of lipids, ions, and water molecules are consistent with the naming scheme of the employed AMBER force fields. In FEW, either the GAFFlipid parameters of Dickson et al. [68] provided in the LipidBook database [97] or the Lipid14 force field [98] available in AMBER 14 [99] can be used for the lipids. If the Lipid14 force field [98] shall be used, we recommend to prepare the PDB file of the solvated membrane bilayer with the CHARMM-GUI Membrane Builder [94–96] because afterwards the script *charmmlipid2amber.py* distributed with AMBER 14 [99] allows an automated conversion of CHARMM to AMBER Lipid14 atom naming. Upon request input files for MD simulations of membrane protein-ligand complexes embedded in an explicit membrane are automatically prepared by FEW for all provided ligand structures. During this preparation, all water molecules located within a user-specified distance to the ligands are removed to avoid clashes. In addition to the files for the MD simulations, batch scripts for easy submission of MD simulation jobs on a compute cluster can be generated. Using the prepared input files MD simulations can be run with the *sander* or *pmemd* programs of AMBER [100].

In the second part of the workflow, MD trajectories of protein-ligand complex systems with an explicit membrane serve as input for the preparation of effective binding energy computations by an implicit solvent/implicit membrane MM-PBSA approach (Fig. 3, top red box). Step 1: Topology files are generated with LEaP using parameter files for the ligands prepared during the setup of the MD simulations by FEW. The topology files contain information about the protein-ligand system as well as Parse radii [101]. We chose Parse radii among the sets of radii available for implicit solvent calculations [101–106] because the Parse radii showed a good performance in a recent extensive study by us on binding free energy calculations for protein–ligand systems [21]. If desired, the radii in the generated files can still be changed by the user prior to starting the calculations, thereby exploiting the gray box character of the calculation setup by FEW. No information about lipids, ions, or water molecules from the MD simulations with an explicit membrane is included in the topology files. The topology files serve as input files for the calculations of the gas phase energy and the nonpolar part of the solvation free energy with the *mm_pbsa.pl* script of AMBER [100]. Step 2: Coordinate files of the snapshots recorded in the MD simulations stripped of lipids, ions, and water molecules are created with *mm_pbsa.pl* for the gas phase and nonpolar solvation free energy calculations. Prior to the snapshot generation, the membrane protein–ligand systems are imaged to the origin, such that the coordinates of the implicit membrane slab can be specified relative to the center of geometry of the membrane protein (see next paragraph). Step 3: PQR files of the same snapshots without lipids, ions, or water molecules are extracted from the MD trajectories. These files are required for the computation of the polar part of the solvation free energies with APBS. Charges for the PQR files are taken from the topology files used for the MD simulations, and radii are assigned according to the Parse radii set [101]. Step 4: All other files required for the implicit solvent/implicit membrane MM-PBSA calculations are automatically created, as are batch files enabling a submission of the MM-PBSA jobs via a queuing system upon request.

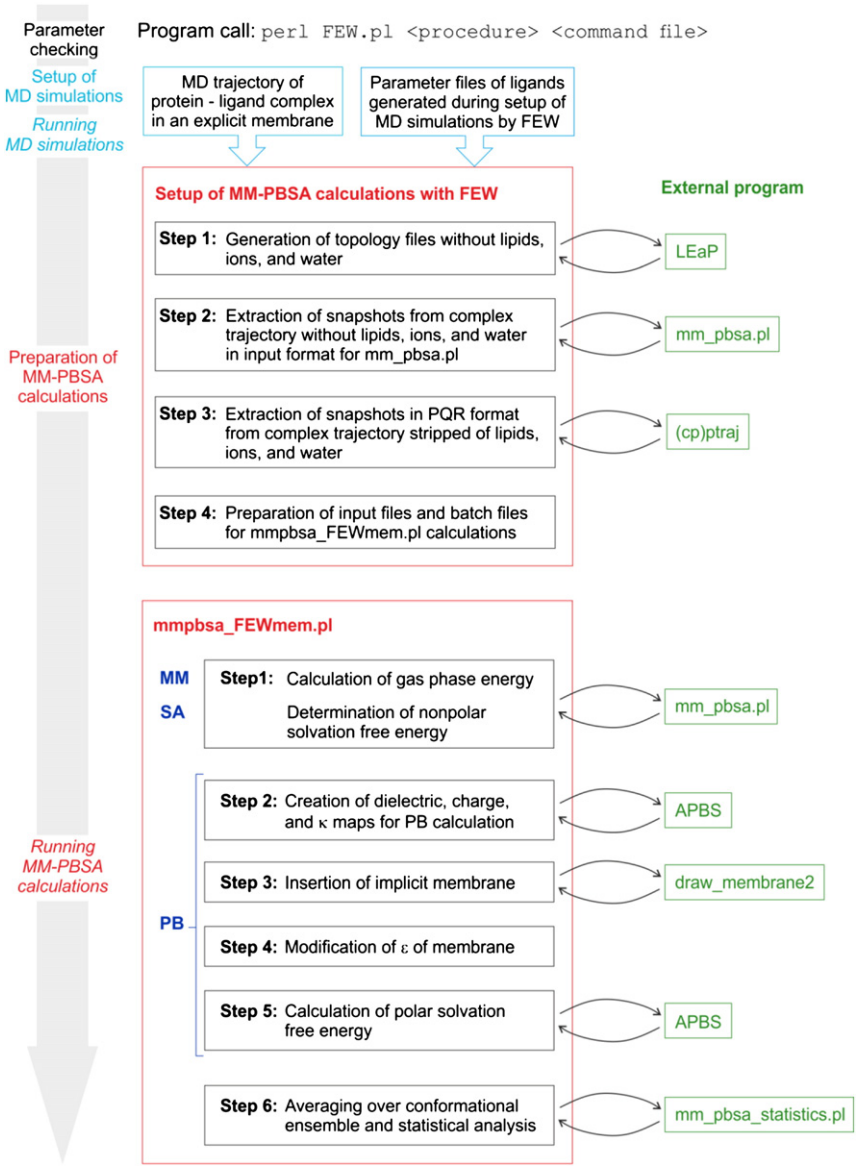

Fig. 3. Workflow of the MM-PBSA procedure (left), schematic depiction (center) of the setup (top red box; using the WAMM module, see Figs. 1 and 3 in Ref. [8]) and execution (bottom red box) of implicit solvent/implicit membrane MM-PBSA calculations by the extended FEW workflow, and used external programs (right). Information required for the setup of the calculations, which is obtained from the preparation and execution of MD simulations in a previous step, is highlighted by light blue boxes.

In the third part of the workflow, the implicit solvent/implicit membrane MM-PBSA calculations are performed by execution of a standalone program provided with FEW called *mmpbsa_FEWmem.pl* (Fig. 3, bottom red box). This program handles the preparation of the input files required for the individual calculation steps and calls the external programs used in the calculation procedure. Step 1: The gas phase energy and the nonpolar part of the solvation free energy of the snapshots in the conformational ensemble are calculated with the *mm_pbsa.pl* script of AMBER [100]. Step 2: Dielectric, charge, and ion accessibility κ maps of the ensemble structures for the computation of the polar part of the solvation free energy are generated with APBS [40]. Step 3: These maps are modified by the *draw_membrane2* [47] program such that an implicit membrane representation is included. The user can specify in the FEW command file the position of the implicit membrane in terms of the lower boundary and the thickness of the membrane slab; if needed, exclusion radii can be defined, too, which allows assigning $\varepsilon_{solvent}$ to the region of the pore in case the protein is a transmembrane channel. Step 4: While *draw_membrane2* by default assigns a dielectric constant of $\varepsilon_{membrane} = 2$ to all points within the membrane region, the uniform assignment in the dielectric maps is modified, if requested, such that a membrane representation comprising up to five slabs with three different dielectric constants results. That way, it is possible to model a membrane with a low dielectric center, embraced on either side by regions of higher dielectric permittivity, which in turn are flanked by regions with a very high dielectric constant. Such a membrane representation is consistent with reported membrane permittivity profiles [107,108]. We note, however, that electrostatic properties of membranes and effects of water at membrane surfaces are complex [107–110]. Consequently, considering the membrane implicitly by a perfectly planar slab, although advantageous with respect to computational costs and convenient with respect to the calculation setup, is a substantial approximation. Step 5: The generated maps are used for computing the polar part of the solvation free energy with APBS [40]. Parameters for the APBS calculations such as the size and resolution of the grid, the solute dielectric constant, and the ion concentration can be specified in the FEW command file (see Ref. [8]). Step 6: The energies computed for the individual snapshots are averaged with the *mm_pbsa_statistics.pl* script of AMBER [100]. In the resulting output file, average values and standard deviations for the gas phase and solvation free energies calculated for complex, receptor, and ligand are provided as are the effective

binding energies. Average effective binding energies and their individual contributions computed for all ligands of a data set can be obtained by calling the *extract_WAMMenergies.pl* script provided with FEW. The thus obtained summary of effective binding energies can be used for a direct comparison of the calculated effective binding energies with experimentally determined binding affinities or for an analysis of the relative binding affinities between pairs of ligands.

In summary, we extended the functionality of FEW such that it can now also be used to prepare and perform effective binding energy calculations by an implicit solvent/implicit membrane MM-PBSA approach for several ligands binding to the same membrane protein. This leads to a considerable speed-up of the preparation step (see below). Furthermore, the *mmpbsa_FEWmem.pl* program now executes several calculation steps requiring different external programs, processes the respective output, and performs a statistical analysis. This greatly reduces the complexity of such analyses.

3.4. Case study — application of the implemented implicit solvent/implicit membrane MM-PBSA calculation procedure

In order to test the implicit solvent/implicit membrane MM-PBSA approach implemented in FEW on a "real-life" data set, we calculated effective binding energies for six ligands (Fig. 4A) that bind to M2TM and thereby block the pore. Such inhibitors have recently re-gained a high interest in drug design to overcome virus resistance against established influenza drugs, such as amantadine (**e**) and rimantadine (**f**). Experimentally measured binding affinities for these compounds have been reported in ref. [56]. In the implemented 1-trajectory MM-PBSA approach, structural rearrangements in the ligand and/or receptor upon binding are not explicitly accounted for, in contrast to the 3-trajectory MM-PBSA approach [58]; furthermore, changes in the configurational entropies of the solutes are not estimated by normal mode [57,58] or quasiharmonic [59] analysis here because such estimates can introduce a considerable uncertainty in the predicted binding affinities [58,91,111,112]. Accordingly, we restricted the data set to compounds that are structurally related to amantadine, which is bound to M2TM in the complex structure that served as a template for the generation of all other complex structures; that way, no large changes in the M2TM or ligand conformation should be expected, and only comparable changes in the configurational entropy upon complex formation should occur. In that case, the computed relative effective binding energies should be a good approximation to the experimental relative binding free energies.

Effective binding energies for the selected ligand compounds were calculated in an automated way applying the implicit solvent/implicit membrane MM-PBSA extension of FEW. The calculations were conducted based on ensembles of 250 snapshots sampled during 5 ns of MD simulations of the M2TM-ligand complexes prepared with FEW. The MD simulations were carried out with *sander* and *pmemd* of AMBER [51] on a compute cluster using 16 CPU cores per M2TM-ligand complex simulation and consumed ~2 days (Table 1). The setup of the six MM-PBSA calculations and the extraction of snapshots from the MD trajectories together took less than 10 min on a workstation (Table 1). The MM-PBSA calculations were run on workstations using one node and one core per ligand and were completed within 1 day (Table 1). Thus, the overall runtime of the calculations amounts to approximately 3 days, which is much faster than rigorous free energy calculations on systems of comparable size: For a system comprising only ~2/3 of the atoms of the M2TM system with explicit membrane, thermodynamic integration calculations consumed more than 2 weeks when 40 cores were used per ligand transformation [8]. Furthermore, the very short setup times for the implicit solvent/implicit membrane MM-PBSA calculations with FEW constitute a considerable speed up of this procedure compared to a manual preparation, which would consume several hours even for an experienced person (Table 1 and Ref.[8]), and due to the automated way, the potential for introducing errors in this step is largely diminished.

The relative effective binding energies computed for the six compounds resulted in a very good ($r^2 = 0.90$) and highly significant ($p < 0.005$) correlation with respect to the experimental relative binding free energies (Fig. 4B). The slope in the correlation line is ~2, showing that the computed effective binding energies overestimate increases in the binding affinity, which may indicate the lack of accounting for enthalpy–entropy compensation [113] even within this series of very similar compounds due to not explicitly considering changes in the configurational entropy upon complex formation. The slope is not considerably affected by using different ε_{solute} values (compare Figs. 4B and S6) because the 1:2 relation between $\Delta\Delta G_{experiment}$ and $\Delta\Delta G_{effective}$ is mainly caused by the van der Waals energy contribution to binding. Only $\Delta\Delta G_{effective}$ of compound **b**, which has a fluorine substituent at the adamantane core, is influenced by ε_{solute}. Consequently, using a three slab model for the membrane with $\varepsilon_{membrane} = 1$ in the region 0–12 Å, $\varepsilon_{membrane} = 3$ in the range 12–18 Å, and $\varepsilon_{membrane} = 160$ in the range 18–25 Å relative to the membrane center also resulted in only marginal differences in the computed $\Delta G_{effective}$ (data not shown). However, in those cases where the effective binding energy

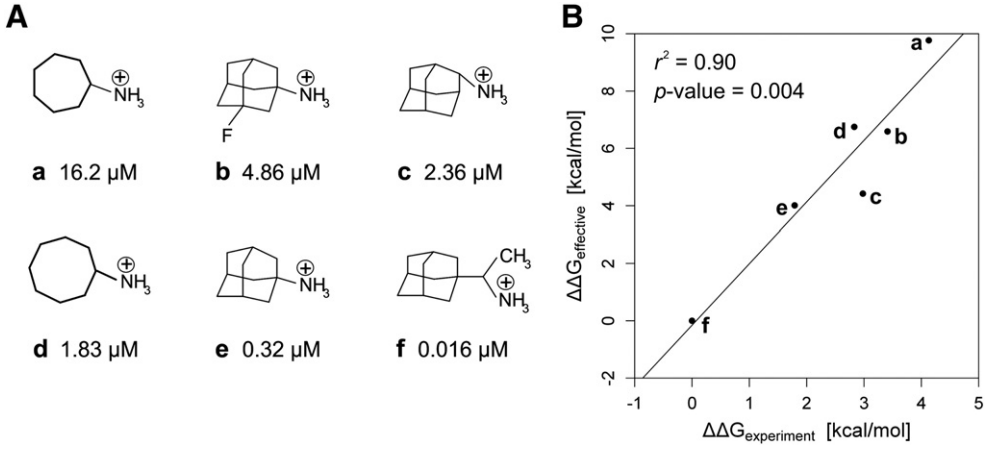

Fig. 4. A: Structures of inhibitors of the M2 proton-channel used for the case study of effective binding energy calculations by the implicit solvent/implicit membrane MM-PBSA approach together with experimentally measured K_d values from Ref. [56]. B: Correlation between computed relative effective binding energies and relative binding free energies derived from experimentally measured K_d values. Experimental binding free energies were calculated according to $\Delta G_{experiment} = -RT \ln(K_d^A/K_d^B)$ with $K_d^A = 1$ M and $T = 300$ K. Compound **f** was used as a reference. The correlation line obtained by a linear least-squares fit is shown as a solid line.

Table 1
Estimates of time required for conducting binding free energy calculations using the extended FEW tool versus performing a purely manual setup.

Task/calculation	No. of ligands [a]	Time with FEW [b,d]	Time for manual setup [c,d]
Generation of command file for preparation of MD simulations with FEW	–[e]	20 min	–[f]
Setup of MD simulations including calculation of RESP charges	6	25 min	5 h
Running equilibration and production MD simulations (16 cores per simulation) [g]	6	2 days	2 days
Generation of command file for setup of MM-PBSA calculations with FEW	–[e]	20 min	–[f]
Setup of MM-PBSA calculations	6	8 min	6 h
Running MM-PBSA calculations (1 core per node and ligand) [h]	6	1 day [i]	3 days [i]

[a] Number of ligands for which the respective setup step/calculation was applied.
[b] Time required when using FEW for the execution of the task/calculation.
[c] Estimate of time needed for a purely manual execution of the task/calculation by an experienced person familiar with the calculation procedure.
[d] Time rounded to days, hours, and minutes.
[e] Number of ligands not relevant.
[f] Task not necessary for a manual setup.
[g] Calculations performed using 16 cores of a multi-node compute cluster with two quadcore Intel Xeon Nehalem 2.4 GHz processors per node.
[h] Calculations were run on workstations with 4 cores using 1 core and 1 workstation per ligand.
[i] The calculation time increases by ~1 day if a more complex representation than the default single slab with $\varepsilon_{membrane} = 2$ is used for the membrane.

of the ligands is dominated by polar contributions, changes in the dielectric constant(s) of the membrane model are expected to have more pronounced effects.

For the calculation with the simple membrane slab with $\varepsilon_{membrane} = 2$ and $\varepsilon_{solute} = 1$ (Fig. 4B) the standard error of the mean was <0.25 kcal mol^{-1} for all compounds, which indicates that sampling structures every 20 ps during 5 ns of MD simulations is sufficient to obtain statistically significant results in this case. It is remarkable that even compounds of pairs with subtle structural modifications are correctly ranked by the computed effective binding energies, e.g., the cycloheptyl (**a**) vs. cyclooctyl (**d**) derivatives, where **d** shows experimentally a ~9-fold higher binding affinity than **a**, amantadine (**e**) vs. its 2-regioisomere (**c**), where the latter shows a ~7-fold decrease of the binding affinity, or amantadine (**e**) vs. rimantadine (**f**), where the latter shows a 20-fold increase of the binding affinity. Thus, although we show results only for one membrane protein–ligand system and on a limited set of compounds, these results indicate that the implicit solvent/implicit membrane MM-PBSA approach implemented in FEW can yield good estimates of relative effective binding energies that may be helpful for, e.g., decision making in the field of rational drug design.

4. Conclusion

We extended the free energy workflow tool FEW, available in AMBER, towards facilitating the setup of MD simulations with an explicit membrane and the setup and execution of effective binding energy calculations according to a 1-trajectory implicit solvent/implicit membrane MM-PBSA approach for multiple ligands binding to the same membrane protein. Our work was motivated by the recent strong increase in the number of high-resolution structures of pharmacologically relevant membrane proteins, the opportunities that arise from this in terms of structure-based drug design, and the lack of any free energy workflow tool specifically developed for such computations. As our extension is embedded in the hierarchical and template-based design of FEW, it requires minimal input information but is still highly adaptable. This should make it interesting for both beginners and experts aiming at implicit solvent/implicit membrane MM-PBSA calculations.

We validated the implemented protocol in three steps. First, by computing the profile of the polar part of the solvation free energy for a sodium ion in the presence of an implicit membrane slab and comparing the results to analytical solutions of the Born equation. Second, by computing the profile of the polar interaction energy of a proton traversing the transmembrane domain of the M2 protein of influenza A. The results are in good qualitative, if not semi-quantitative, agreement for several important events along the proton pathway with those obtained in a study applying much more sophisticated computational techniques. Finally, we performed a case study on effective binding energy calculations according to the implemented implicit solvent/implicit membrane MM-PBSA approach for a set of inhibitors of M2TM. We estimated a considerable speed up in the setup and analysis times for the implicit solvent/implicit membrane MM-PBSA calculations by FEW compared to a manual preparation. Together with the overall runtime of the calculations and the results of the sample analysis, this suggests that such type of calculations can be valuable for estimating relative effective binding energies in later stages of drug design projects on membrane proteins. As the extended version of FEW reduces the effort and complexity in setting up such calculations, we think that it will help to pursue such studies with the AMBER package.

Acknowledgements

We are grateful to A. Kolocouris, National and Kapodistrian University of Athens, for pointing us to the interesting M2 protein channel of the influenza A virus and the "Zentrum für Informations- und Medientechnologie" (ZIM) at the Heinrich-Heine-University Düsseldorf for the computational support. We are grateful to the Deutscher Akademischer Austauschdienst (DAAD) for financial support within the IKYDA program. The source code of the extended version of FEW together with template command and input files will be made available within the AMBER package of molecular simulation programs.

Appendix A. Supplementary data

Supplementary data to this article can be found online at http://dx.doi.org/10.1016/j.bbagen.2014.10.013.

References

[1] M. Sällman Almén, K.J.V. Nordström, R. Fredriksson, H.B. Schiöth, Mapping the human membrane proteome: a majority of the human membrane proteins can be classified according to function and evolutionary origin, BMC Biol. 7 (2009) 50, http://dx.doi.org/10.1186/1741-7007-7-50.
[2] Y. Arinaminpathy, E. Khurana, D.M. Engelman, M.B. Gerstein, Computational analysis of membrane proteins: the largest class of drug targets, Drug Discov. Today 14 (2009) 1130–1135, http://dx.doi.org/10.1016/j.drudis.2009.08.006.
[3] M.A. Yildirim, K.I. Goh, M.E. Cusick, A.L. Barabási, M. Vidal, Drug-target network, Nat. Biotechnol. 25 (2007) 1119–1126, http://dx.doi.org/10.1038/nbt1338.
[4] M. Baker, Making membrane proteins for structures: a trillion tiny tweaks, Nat. Methods 7 (2010) 429–434, http://dx.doi.org/10.1038/nmeth0610-429.
[5] V. Katritch, V. Cherezov, R.C. Stevens, Structure-function of the G protein-coupled receptor superfamily, Annu. Rev. Pharmacol. Toxicol. 53 (2013) 531–556, http://dx.doi.org/10.1146/annurev-pharmtox-032112-135923.
[6] G. Fernández-Ballester, A. Fernández-Carvajal, J.M. González-Ros, A. Ferrer-Montiel, Ionic channels as targets for drug design: a review on computational methods, Pharmaceutics 3 (2011) 932–953, http://dx.doi.org/10.3390/pharmaceutics3040932.
[7] J.W.F. Robertson, J.J. Kasianowicz, S. Banerjee, Analytical approaches for studying transporters, channels and porins, Chem. Rev. 112 (2012) 6227–6249, http://dx.doi.org/10.1021/cr300317z.

[8] N. Homeyer, H. Gohlke, FEW: a workflow tool for free energy calculations of ligand binding, J. Comput. Chem. 34 (2012) 965–973, http://dx.doi.org/10.1002/jcc.23218.
[9] W.L. Jorgensen, The many roles of computation in drug discovery, Science 303 (2004) 1813–1818, http://dx.doi.org/10.1126/science.1096361.
[10] M.K. Gilson, H.X. Zhou, Calculation of protein–ligand binding affinities, Annu. Rev. Biophys. Biomol. Struct. 36 (2007) 21–42, http://dx.doi.org/10.1146/annurev.biophys.36.040306.132550.
[11] E. Stjernschantz, C. Oostenbrink, Improved ligand–protein binding affinity predictions using multiple binding modes, Biophys. J. 98 (2010) 2682–2691, http://dx.doi.org/10.1016/j.bpj.2010.02.034.
[12] G.L. Warren, C.W. Andrews, A.M. Capelli, B. Clarke, J. LaLonde, M.H. Lambert, M. Lindvall, N. Nevins, S.F. Semus, S. Senger, G. Tedesco, I.D. Wall, J.M. Woolven, C.E. Peishoff, M.S. Head, A critical assessment of docking programs and scoring functions, J. Med. Chem. 49 (2006) 5912–5931, http://dx.doi.org/10.1021/jm050362n.
[13] J. Michel, J.W. Essex, Prediction of protein–ligand binding affinity by free energy simulations: assumptions, pitfalls and expectations, J. Comput. Aided Mol. Des. 24 (2010) 639–658, http://dx.doi.org/10.1007/s10822-010-9363-3.
[14] O. Acevedo, Z. Ambrose, P.T. Flaherty, H. Aamer, P. Jain, S.V. Sambasivarao, Identification of HIV inhibitors guided by free energy perturbation calculations, Curr. Pharm. Des. 18 (2012) 1199–1216.
[15] J. Åqvist, V.B. Luzhkov, B.O. Brandsdal, Ligand binding affinities from MD simulations, Acc. Chem. Res. 35 (2002) 358–365, http://dx.doi.org/10.1021/ar010014p.
[16] J. Åqvist, C. Medina, J.E. Samuelsson, A new method for predicting binding affinity in computer-aided drug design, Protein Eng. 7 (1994) 385–391, http://dx.doi.org/10.1093/protein/7.3.385.
[17] N. Homeyer, H. Gohlke, Free energy calculations by the molecular mechanics Poisson–Boltzmann surface area method, Mol. Inf. 31 (2012) 114–122, http://dx.doi.org/10.1002/minf.201100135.
[18] Y.Y. Sham, Z.T. Chu, H. Tao, A. Warshel, Examining methods for calculations of binding free energies: LRA, LIE, PDLD-LRA, and PDLD/S-LRA calculations of ligands binding to an HIV protease, Proteins Struct. Funct. Genet. 39 (2000) 393–407.
[19] S. Huo, J. Wang, P. Cieplak, P.A. Kollman, I.D. Kuntz, Molecular dynamics and free energy analyses of cathepsin D-inhibitor interactions: insight into structure-based ligand design, J. Med. Chem. 45 (2002) 1412–1419, http://dx.doi.org/10.1021/jm010338j.
[20] T. Yang, J.C. Wu, C. Yan, Y. Wang, R. Luo, M.B. Gonzales, K.N. Dalby, P. Ren, Virtual screening using molecular simulations, Proteins Struct. Funct. Genet. 79 (2011) 1940–1951, http://dx.doi.org/10.1002/prot.23018.
[21] N. Homeyer, F. Stoll, A. Hillisch, H. Gohlke, Binding free energy calculations for lead optimization: assessment of their accuracy in an industrial drug design context, J. Chem. Theory Comput. 10 (2014) 3331–3344, http://dx.doi.org/10.1021/ct5000296.
[22] L. Xu, H. Sun, Y. Li, J. Wang, T. Hou, Assessing the performance of MM/PBSA and MM/GBSA methods. 3. The impact of force fields and ligand charge models, J. Phys. Chem. B 117 (2013) 8408–8421, http://dx.doi.org/10.1021/jp404160y.
[23] S. Liu, Y. Wu, T. Lin, R. Abel, J.P. Redmann, C.M. Summa, V.R. Jaber, N.M. Lim, D.L. Mobley, Lead optimization mapper: automating free energy calculations for lead optimization, J. Comput. Aided Mol. Des. 27 (2013) 755–770, http://dx.doi.org/10.1007/s10822-013-9678-y.
[24] M.A. Lill, M.L. Danielson, Computer-aided drug design platform using PyMOL, J. Comput. Aided Mol. Des. 25 (2011) 13–19, http://dx.doi.org/10.1007/s10822-010-9395-8.
[25] MCPRO+, version 3.2, Schrödinger, LLC, New York, NY, 2013.
[26] Desmond Molecular Dynamics System, version 3.7, D. E. Shaw Research, New York, NY, 2014.
[27] Maestro-Desmond Interoperability Tools, version 3.7, Schrodinger, New York, NY, 2014.
[28] K.J. Bowers, E. Chow, H. Xu, R.O. Dror, M.P. Eastwood, B.A. Gregersen, J.L. Klepeis, I. Kolossváry, M.A. Moraes, F.D. Sacerdoti, J.K. Salmon, Y. Shan, D.E. Shaw, Scalable algorithms for molecular dynamics simulations on commodity clusters, Proceedings of the ACM/IEEE Conference on Supercomputing (SC06), 2006 (Tampa, Florida).
[29] D. Shivakumar, J. Williams, Y. Wu, W. Damm, J. Shelley, W. Sherman, Prediction of absolute solvation free energies using molecular dynamics free energy perturbation and the OPLS force field, J. Chem. Theory Comput. 6 (2010) 1509–1519, http://dx.doi.org/10.1021/ct900587b.
[30] S. Jo, W. Jiang, H.S. Lee, B. Roux, W. Im, CHARMM-GUI Ligand Binder for absolute binding free energy calculations and its application, J. Chem. Inf. Model. 53 (2013) 267–277, http://dx.doi.org/10.1021/ci300505n.
[31] G. Rastelli, G. Degliesposti, A. Del Rio, M. Sgobba, Binding estimation after refinement: a new automated procedure for the refinement and rescoring of docked ligands in virtual screening, Chem. Biol. Drug Des. 73 (2009) 283–286, http://dx.doi.org/10.1111/j.1747-0285.2009.00780.x.
[32] H.I. Ingólfsson, C.A. Lopez, J.J. Uusitalo, D.H. de Jong, S.M. Gopal, X. Periole, S.J. Marrink, The power of coarse graining in biomolecular simulations, Wiley Interdiscip, Rev. Comput. Mol. Sci. 4 (2014) 225–248, http://dx.doi.org/10.1002/wcms.1169.
[33] A. Grossfield, Implicit modeling of membranes, in: S. Feller (Ed.), Current Topics in Membranes, Comput. Model. Membr., vol. 60, Elsevier Inc., 2008, http://dx.doi.org/10.1016/S1063-5823(08)00005-7.
[34] J. Kleinjung, F. Fraternali, Design and application of implicit solvent models in biomolecular simulations, Curr. Opin. Struct. Biol. 25 (2014) 126–134, http://dx.doi.org/10.1016/j.sbi.2014.04.003.
[35] Y. He, L. Prieto, T. Lazaridis, Modeling peptide binding to anionic membrane pores, J. Comput. Chem. 34 (2013) 1463–1475, http://dx.doi.org/10.1002/jcc.23282.
[36] W. Rocchia, E. Alexov, B. Honig, Extending the applicability of the nonlinear Poisson–Boltzmann equation: multiple dielectric constants and multivalent ions, J. Phys. Chem. B 105 (2001) 6507–6514, http://dx.doi.org/10.1021/jp010454y.
[37] W.M. Botello-Smith, X. Liu, Q. Cai, Z. Li, H. Zhao, R. Luo, Numerical Poisson–Boltzmann model for continuum membrane systems, Chem. Phys. Lett. 555 (2013) 274–281, http://dx.doi.org/10.1016/j.cplett.2012.10.081.
[38] W. Im, D. Beglov, B. Roux, Continuum solvation model: computation of electrostatic forces from numerical solutions to the Poisson–Boltzmann equation, Comput. Phys. Commun. 111 (1998) 59–75, http://dx.doi.org/10.1016/S0010-4655(98)00016-2.
[39] V. Jogini, B. Roux, Electrostatics of the intracellular vestibule of K^+ channels, J. Mol. Biol. 354 (2005) 272–288, http://dx.doi.org/10.1016/j.jmb.2005.09.031.
[40] N.A. Baker, D. Sept, S. Joseph, M.J. Holst, J.A. McCammon, Electrostatics of nanosystems: application to microtubules and the ribosome, Proc. Natl. Acad. Sci. U. S. A. 98 (2001) 10037–10041, http://dx.doi.org/10.1073/pnas.181342398.
[41] K.M. Callenberg, O.P. Choudhary, G.L. de Forest, D.W. Gohara, N.A. Baker, M. Grabe, APBSmem: a graphical interface for electrostatic calculations at the membrane, PLoS ONE 5 (2010) e12722, http://dx.doi.org/10.1371/journal.pone.0012722.
[42] N. Smith, B. Campbell, L. Li, C. Li, E. Alexov, Protein Nano-Object Integrator (ProNOI) for generating atomic style objects for molecular modeling, BMC Struct. Biol. 12 (2012) 31, http://dx.doi.org/10.1186/1472-6807-12-31.
[43] T. Kimmett, N. Smith, S. Witham, M. Petukh, S. Sarkar, E. Alexov, ProBLM Web Server: protein and membrane placement and orientation package, Comput. Math. Methods Med. (2014) 1–7, http://dx.doi.org/10.1155/2014/838259.
[44] S. Jo, M. Vargyas, J. Vasko-Szedlar, B. Roux, W. Im, PBEQ-Solver for online visualization of electrostatic potential of biomolecules, Nucleic Acids Res. 36 (2008) W270–W275, http://dx.doi.org/10.1093/nar/gkn314.
[45] M. Holst, F. Saied, Multigrid solution of the Poisson–Boltzmann equation, J. Comput. Chem. 14 (1993) 105–113, http://dx.doi.org/10.1002/jcc.540140114.
[46] M.J. Holst, F. Saied, Numerical solution of the nonlinear Poisson–Boltzmann equation: developing more robust and efficient methods, J. Comput. Chem. 16 (1995) 337–364, http://dx.doi.org/10.1002/jcc.540160308.
[47] M. Grabe, draw_membrane2, 2008. (Pittsburgh, PA, USA).
[48] M.K. Gilson, B. Honig, Calculation of the total electrostatic energy of a macromolecular system: solvation energies, binding energies, and conformational analysis, Proteins Struct. Funct. Genet. 4 (1988) 7–18, http://dx.doi.org/10.1002/prot.340040104.
[49] H.M. Berman, J. Westbrook, Z. Feng, G. Gilliland, T.N. Bhat, H. Weissig, I.N. Shindyalov, P.E. Bourne, The Protein Data Bank, Nucleic Acids Res. 28 (2000) 235–242, http://dx.doi.org/10.1093/nar/28.1.235.
[50] A.L. Stouffer, R. Acharya, D. Salom, A.S. Levine, L. Di Costanzo, C.S. Soto, V. Tereshko, V. Nanda, S. Stayrook, W.F. DeGrado, Structural basis for the function and inhibition of an influenza virus proton channel, Nature 451 (2008) 596–599, http://dx.doi.org/10.1038/nature06528.
[51] D.A. Case, T.A. Darden, T.E. Cheatham III, C.L. Simmerling, J. Wang, R.E. Duke, R. Luo, R.C. Walker, W. Zhang, K.M. Merz, B. Roberts, S. Hayik, A. Roitberg, G. Seabra, J. Swails, A.W. Götz, I. Kolossváry, K.F. Wong, F. Paesani, J. Vanicek, R.M. Wolf, J. Liu, X. Wu, S.R. Brozell, T. Steinbrecher, H. Gohlke, Q. Cai, X. Ye, J. Wang, M.-J. Hsieh, G. Cui, D.R. Roe, D.H. Mathews, M.G. Seetin, R. Salomon-Ferrer, C. Sagui, V. Babin, T. Luchko, S. Gusarov, A. Kovalenko, P.A. Kollman, AMBER 12, University of California, San Francisco, 2012.
[52] B.R. Miller III, T.D. McGee Jr., J.M. Swails, N. Homeyer, H. Gohlke, A.E. Roitberg, MMPBSA.py: an efficient program for end-state free energy calculations, J. Chem. Theory Comput. 8 (2012) 3314–3321, http://dx.doi.org/10.1021/ct300418h.
[53] W.D. Cornell, P. Cieplak, C.I. Bayly, I.R. Gould, K.M. Merz, D.M. Ferguson, D.C. Spellmeyer, T. Fox, J.W. Caldwell, P.A. Kollman, A second generation force field for the simulation of proteins, nucleic acids, and organic molecules, J. Am. Chem. Soc. 117 (1995) 5179–5197, http://dx.doi.org/10.1021/ja00124a002.
[54] V. Hornak, R. Abel, A. Okur, B. Strockbine, A. Roitberg, C. Simmerling, Comparison of multiple Amber force fields and development of improved protein backbone parameters, Proteins Struct. Funct. Genet. 65 (2006) 712–725, http://dx.doi.org/10.1002/prot.21123.
[55] M.A. Lomize, A.L. Lomize, I.D. Pogozheva, H.I. Mosberg, OPM: orientations of proteins in membranes database, Bioinformatics 22 (2006) 623–625, http://dx.doi.org/10.1093/bioinformatics/btk023.
[56] S. Eleftheratos, P. Spearpoint, G. Ortore, A. Kolocouris, A. Martinelli, S. Martin, A. Hay, Interaction of aminoadamantane derivatives with the influenza A virus M2 channel-docking using a pore blocking model, Bioorg. Med. Chem. Lett. 20 (2010) 4182–4187, http://dx.doi.org/10.1016/j.bmcl.2010.05.049.
[57] J. Srinivasan, T.E. Cheatham III, P. Cieplak, P.A. Kollman, D.A. Case, Continuum solvent studies of the stability of DNA, RNA, and Phosphoramidate–DNA helices, J. Am. Chem. Soc. 120 (1998) 9401–9409, http://dx.doi.org/10.1021/ja981844.
[58] H. Gohlke, D.A. Case, Converging free energy estimates: MM-PB(GB)SA studies on the protein–protein complex Ras–Raf, J. Comput. Chem. 25 (2004) 238–250, http://dx.doi.org/10.1002/jcc.10379.
[59] M. Karplus, J.N. Kushick, Method for estimating the configurational entropy of macromolecules, Macromolecules 14 (1981) 325–332, http://dx.doi.org/10.1021/ma50003a019.
[60] S.D. Cady, K. Schmidt-Rohr, J. Wang, C.S. Soto, W.F. DeGrado, M. Hong, Structure of the amantadine binding site of influenza M2 proton channels in lipid bilayers, Nature 463 (2010) 689–692, http://dx.doi.org/10.1038/nature08722.
[61] J. Hu, R. Fu, T.A. Cross, The chemical and dynamical influence of the anti-viral drug amantadine on the M2 proton channel transmembrane domain, Biophys. J. 93 (2007) 276–283, http://dx.doi.org/10.1529/biophysj.106.102103.
[62] F. Hu, W. Luo, M. Hong, Mechanisms of proton conduction and gating in influenza M2 proton channels from solid-state NMR, Science 330 (2010) 505–508, http://dx.doi.org/10.1126/science.1191714.
[63] H. Dong, G. Fiorin, W.F. DeGrado, M.L. Klein, Exploring histidine conformations in the M2 channel lumen of the influenza A virus at neutral pH via molecular simulations, J. Phys. Chem. Lett. 4 (2013) 3067–3071, http://dx.doi.org/10.1021/jz401672h.

[64] R. Acharya, V. Carnevale, G. Fiorin, B.G. Levine, A.L. Polishchuk, V. Balannik, I. Samish, R.A. Lamb, L.H. Pinto, W.F. DeGrado, M.L. Klein, Structure and mechanism of proton transport through the transmembrane tetrameric M2 protein bundle of the influenza A virus, Proc. Natl. Acad. Sci. U. S. A. 107 (2010) 15075–15080, http://dx.doi.org/10.1073/pnas.1007071107.

[65] D.A. Case, T.A. Darden, T.E. Cheatham III, C.L. Simmerling, J. Wang, R.E. Duke, R. Luo, R.C. Walker, W. Zhang, K.M. Merz, B. Roberts, S. Hayik, A. Roitberg, G. Seabra, J. Swails, A.W. Götz, I. Kolossváry, K.F. Wong, F. Paesani, J. Vanicek, R.M. Wolf, J. Liu, X. Wu, S.R. Brozell, T. Steinbrecher, H. Gohlke, Q. Cai, X. Ye, J. Wang, M.-J. Hsieh, G. Cui, D.R. Roe, D.H. Mathews, M.G. Seetin, R. Salomon-Ferrer, C. Sagui, V. Babin, T. Luchko, S. Gusarov, A. Kovalenko, P.A. Kollman, AmberTools 12, University of California, San Francisco, 2012.

[66] I.S. Joung, T.E. Cheatham III, Determination of alkali and halide monovalent ion parameters for use in explicitly solvated biomolecular simulations, J. Phys. Chem. B 112 (2008) 9020–9041, http://dx.doi.org/10.1021/jp8001614.

[67] I.S. Joung, T.E. Cheatham III, Molecular dynamics simulations of the dynamic and energetic properties of alkali and halide ions using water-model-specific ion parameters, J. Phys. Chem. B 113 (2009) 13279–13290, http://dx.doi.org/10.1021/jp902584c.

[68] C.J. Dickson, L. Rosso, R.M. Betz, R.C. Walker, I.R. Gould, GAFFlipid: a General Amber Force Field for the accurate molecular dynamics simulation of phospholipid, Soft Matter 8 (2012) 9617–9627, http://dx.doi.org/10.1039/C2SM26007G.

[69] C.I. Bayly, P. Cieplak, W.D. Cornell, P.A. Kollman, A well-behaved electrostatic potential based method using charge restraints for deriving atomic charges: the RESP model, J. Phys. Chem. 97 (1993) 10269–10280, http://dx.doi.org/10.1021/j100142a004.

[70] M.J. Frisch, G.W. Trucks, H.B. Schlegel, G.E. Scuseria, M.A. Robb, J.R. Cheeseman, J.A. Montgomery Jr., T. Vreven, K.N. Kudin, J.C. Burant, J.M. Millam, S.S. Iyengar, J. Tomasi, V. Barone, B. Mennucci, M. Cossi, G. Scalmani, N. Rega, G.A. Petersson, H. Nakatsuji, M. Hada, M. Ehara, K. Toyota, R. Fukuda, J. Hasegawa, M. Ishida, T. Nakajima, Y. Honda, O. Kitao, H. Nakai, M. Klene, X. Li, J.E. Knox, H.P. Hratchian, J.B. Cross, V. Bakken, C. Adamo, J. Jaramillo, R. Gomperts, R.E. Stratmann, O. Yazyev, A.J. Austin, R. Cammi, C. Pomelli, J.W. Ochterski, P.Y. Ayala, K. Morokuma, G.A. Voth, P. Salvador, J.J. Dannenberg, V.G. Zakrzewski, S. Dapprich, A.D. Daniels, M.C. Strain, O. Farkas, D.K. Malick, A.D. Rabuck, K. Raghavachari, J.B. Foresman, J.V. Ortiz, Q. Cui, A.G. Baboul, S. Clifford, J. Cioslowski, B.B. Stefanov, G. Liu, A. Liashenko, P. Piskorz, I. Komaromi, R.L. Martin, D.J. Fox, T. Keith, M.A. Al-Laham, C.Y. Peng, A. Nanayakkara, M. Challacombe, P.M.W. Gill, B. Johnson, W. Chen, M.W. Wong, C. Gonzalez, J.A. Pople, Gaussian 03, Revision D.01, Gaussian, Inc., Wallingford CT, 2004.

[71] J. Wang, R.M. Wolf, J.W. Caldwell, P.A. Kollman, D.A. Case, Development and testing of a general Amber force field, J. Comput. Chem. 25 (2004) 1157–1174, http://dx.doi.org/10.1002/jcc.20035.

[72] D.R. Roe, T.E. Cheatham III, PTRAJ and CPPTRAJ: software for processing and analysis of molecular dynamics trajectory data, J. Chem. Theory Comput. 9 (2013) 3084–3095, http://dx.doi.org/10.1021/ct400341p.

[73] H. Loeffler, Handy routines for Ptraj/Cpptraj, CSE, Daresbury, UK, 2012. (http://www.hecbiosim.ac.uk/ptraj-routines).

[74] The PyMOL Molecular Graphics System, Version 1.3, Schrödinger, LLC, 2011.

[75] T. Williams, C. Kelley, et al., Gnuplot 4.6: an interactive plotting program, http://gnuplot.sourceforge.net2012.

[76] Grace Development Team, Grace, version 5.1.22, http://plasma-gate.weizmann.ac.il/Grace/.

[77] SYBYL-X 1.2, Tripos International 1699 South Hanley Rd., St. Louis, Missouri, 63144, USA2010.

[78] MOLOC, Roche Biostructural Community, 2008. (http://www.moloc.ch, April).

[79] P.R. Gerber, K. Müller, MAB, a generally applicable molecular force field for structure modelling in medicinal chemistry, J. Comput. Aided Mol. Des. 9 (1995) 251–268, http://dx.doi.org/10.1007/BF00124456.

[80] P.R. Gerber, Charge distribution from a simple molecular orbital type calculation and non-bonding interaction terms in the force field MAB, J. Comput. Aided Mol. Des. 12 (1998) 37–51, http://dx.doi.org/10.1023/A:1007902804814.

[81] ROCS 3.2.0.4, OpenEye Scientific Software, Santa Fe, NM, http://www.eyesopen.com.

[82] P.C.D. Hawkins, A.G. Skillman, A. Nicholls, Comparison of shape-matching and docking as virtual screening tools, J. Med. Chem. 50 (2007) 74–82, http://dx.doi.org/10.1021/jm0603365.

[83] M.J. Frisch, G.W. Trucks, H.B. Schlegel, G.E. Scuseria, M.A. Robb, J.R. Cheeseman, G. Scalmani, V. Barone, B. Mennucci, G.A. Petersson, H. Nakatsuji, M. Caricato, X. Li, H.P. Hratchian, A.F. Izmaylov, J. Bloino, G. Zheng, J.L. Sonnenberg, M. Hada, M. Ehara, K. Toyota, R. Fukuda, J. Hasegawa, M. Ishida, T. Nakajima, Y. Honda, O. Kitao, H. Nakai, T. Vreven, J.A. Montgomery Jr., J.E. Peralta, F. Ogliaro, M. Bearpark, J.J. Heyd, E. Brothers, K.N. Kudin, V.N. Staroverov, R. Kobayashi, J. Normand, K. Raghavachari, A. Rendell, J.C. Burant, S.S. Iyengar, J. Tomasi, M. Cossi, N. Rega, J.M. Millam, M. Klene, J.E. Knox, J.B. Cross, V. Bakken, C. Adamo, J. Jaramillo, R. Gomperts, R.E. Stratmann, O. Yazyev, A.J. Austin, R. Cammi, C. Pomelli, J.W. Ochterski, R.L. Martin, K. Morokuma, V.G. Zakrzewski, G.A. Voth, P. Salvador, J.J. Dannenberg, S. Dapprich, A.D. Daniels, Ö. Farkas, J.B. Foresman, J.V. Ortiz, J. Cioslowski, D.J. Fox, Gaussian 09, Revision A.02, 2009.

[84] R Core Team, R: a language and environment for statistical computing, R Foundation for Statistical Computing, Vienna, Austria, 2010. http://www.R-project.org.

[85] R. Liang, H. Li, J.M.J. Swanson, G.A. Voth, Multiscale simulation reveals a multifaceted mechanism of proton permeation through the influenza A M2 proton channel, Proc. Natl. Acad. Sci. U. S. A. 111 (2014) 9396–9401, http://dx.doi.org/10.1073/pnas.1401997111.

[86] Y. Marcus, Volumes of aqueous hydrogen and hydroxide ions at 0 to 200 °C, J. Chem. Phys. 137 (2012) 154501, http://dx.doi.org/10.1063/1.4758071.

[87] J. Wang, J.X. Qiu, C. Soto, W.F. DeGrado, Structural and dynamic mechanisms for the function and inhibition of the M2 proton channel from influenza A virus, Curr. Opin. Struct. Biol. 21 (2011) 68–80, http://dx.doi.org/10.1016/j.sbi.2010.12.002.

[88] J. Hu, R. Fu, K. Nishimura, L. Zhang, H.X. Zhou, D.D. Busath, V. Vijayvergiya, T.A. Cross, Histidines, heart of the hydrogen ion channel from influenza A virus: toward an understanding of conductance and proton selectivity, Proc. Natl. Acad. Sci. U. S. A. 103 (2006) 6865–6870, http://dx.doi.org/10.1073/pnas.0601944103.

[89] F. Hu, K. Schmidt-Rohr, M. Hong, NMR detection of pH-dependent histidine-water proton exchange reveals the conduction mechanism of a transmembrane proton channel, J. Am. Chem. Soc. 134 (2012) 3703–3713, http://dx.doi.org/10.1021/ja2081185.

[90] P. Kukic, D. Farrell, L.P. McIntosh, B. García-Moreno, E.K.S. Jensen, Z. Toleikis, K. Teilum, J.E. Nielsen, Protein dielectric constants determined from NMR chemical shift perturbations, J. Am. Chem. Soc. 135 (2013) 16968–16976, http://dx.doi.org/10.1021/ja406995j.

[91] T. Hou, J. Wang, Y. Li, W. Wang, Assessing the performance of the MM/PBSA and MM/GBSA methods. 1. The accuracy of binding free energy calculations based on molecular dynamics simulations, J. Chem. Inf. Model. 51 (2011) 69–82, http://dx.doi.org/10.1021/ci100275a.

[92] T.C. Berkelbach, H.S. Lee, M.E. Tuckerman, Concerted hydrogen-bond dynamics in the transport mechanism of the hydrated proton: a first-principles molecular dynamics study, Phys. Rev. Lett. 103 (2009) 238302, http://dx.doi.org/10.1103/PhysRevLett.103.238302.

[93] H. Lapid, N. Agmon, M.K. Petersen, G.A. Voth, A bond-order analysis of the mechanism for hydrated proton mobility in liquid water, J. Chem. Phys. 122 (2005) 14506, http://dx.doi.org/10.1063/1.1814973.

[94] S. Jo, T. Kim, W. Im, Automated builder and database of protein/membrane complexes for molecular dynamics simulations, PLoS ONE 2 (2007) e880, http://dx.doi.org/10.1371/journal.pone.0000880.

[95] S. Jo, J.B. Lim, J.B. Klauda, W. Im, CHARMM-GUI Membrane Builder for mixed bilayers and its application to yeast membranes, Biophys. J. 97 (2009) 50–58, http://dx.doi.org/10.1016/j.bpj.2009.04.013.

[96] E.L. Wu, X. Cheng, S. Jo, H. Rui, K.C. Song, E.M. Dávila-Contreras, Y. Qi, J. Lee, V. Monje-Galvan, R.M. Venable, J.B. Klauda, W. Im, CHARMM-GUI Membrane Builder toward realistic biological membrane simulations, J. Comput. Chem. 35 (2014) 1997–2004, http://dx.doi.org/10.1002/jcc.23702.

[97] J. Domanski, P.J. Stansfeld, M.S.P. Sansom, O. Beckstein, Lipidbook: a public repository for force-field parameters used in membrane simulations, J. Membr. Biol. 236 (2010) 255–258, http://dx.doi.org/10.1007/s00232-010-9296-8.

[98] C.J. Dickson, B.D. Madej, A.A. Skjevik, R.M. Betz, K. Teigen, I.R. Gould, R.C. Walker, Lipid14: the Amber lipid force field, J. Chem. Theory Comput. 10 (2014) 865–879, http://dx.doi.org/10.1021/ct4010307.

[99] D.A. Case, V. Babin, J.T. Berryman, R.M. Betz, Q. Cai, D.S. Cerutti, T.E. Cheatham III, T.A. Darden, R.E. Duke, H. Gohlke, A.W. Goetz, S. Gusarov, N. Homeyer, P. Janowski, J. Kaus, I. Kolossváry, A. Kovalenko, T.S. Lee, S. LeGrand, T. Luchko, R. Luo, B. Madej, K.M. Merz, F. Paesani, D.R. Roe, A. Roitberg, C. Sagui, R. Salomon-Ferrer, G. Seabra, C.L. Simmerling, W. Smith, J. Swails, R.C. Walker, J. Wang, R.M. Wolf, X. Wu, P.A. Kollman, AMBER 14, University of California, San Francisco, 2014.

[100] D.A. Case, T.E. Cheatham III, T. Darden, H. Gohlke, R. Luo, K.M. Merz Jr., A. Onufriev, C. Simmerling, B. Wang, R.J. Woods, The Amber biomolecular simulation programs, J. Comput. Chem. 26 (2005) 1668–1688, http://dx.doi.org/10.1002/jcc.20290.

[101] D. Sitkoff, K.A. Sharp, B. Honig, Accurate calculation of hydration free energies using macroscopic solvent models, J. Phys. Chem. 98 (1994) 1978–1988, http://dx.doi.org/10.1021/j100058a043.

[102] J.M.J. Swanson, S.A. Adcock, J.A. McCammon, Optimized radii for Poisson–Boltzmann calculations with the AMBER force field, J. Chem. Theory Comput. 1 (2005) 484–493, http://dx.doi.org/10.1021/ct049834o.

[103] C. Tan, L. Yang, R. Luo, How well does Poisson–Boltzmann implicit solvent agree with explicit solvent? A quantitative analysis, J. Phys. Chem. B 110 (2006) 18680–18687, http://dx.doi.org/10.1021/jp063479b.

[104] V. Tsui, D.A. Case, Molecular dynamics simulations of nucleic acids with a generalized Born solvation model, J. Am. Chem. Soc. 122 (2000) 2489–2498, http://dx.doi.org/10.1021/ja9939385.

[105] V. Tsui, D.A. Case, Theory and applications of the generalized Born solvation model in macromolecular simulations, Biopolymers 56 (2000) 275–291.

[106] M. Nina, D. Beglov, B. Roux, Atomic radii for continuum electrostatics calculations based on molecular dynamics free energy simulations, J. Phys. Chem. 101 (1997) 5239–5248, http://dx.doi.org/10.1021/jp970736r.

[107] H. Nymeyer, H.X. Zhou, A method to determine dielectric constants in nonhomogeneous systems: application to biological membranes, Biophys. J. 94 (2008) 1185–1193, http://dx.doi.org/10.1529/biophysj.107.117770.

[108] H.A. Stern, S.E. Feller, Calculation of the dielectric permittivity profile for a nonuniform system: application to a lipid bilayer simulation, J. Chem. Phys. 118 (2003) 3401–3412, http://dx.doi.org/10.1063/1.1537244.

[109] H.E. Alper, D. Bassolino-Klimas, T.R. Stouch, The limiting behavior of water hydrating a phospholipid monolayer: a computer simulation study, J. Chem. Phys. 99 (1993) 5547–5559, http://dx.doi.org/10.1063/1.465947.

[110] J.H. Lin, N.A. Baker, J.A. McCammon, Bridging implicit and explicit solvent approaches for membrane electrostatics, Biophys. J. 83 (2002) 1374–1379, http://dx.doi.org/10.1016/S0006-3495(02)73908-8.

[111] A. Weis, K. Katebzadeh, P. Söderhjelm, I. Nilsson, U. Ryde, Ligand affinities predicted with the MM/PBSA method: dependence on the simulation method and the force field, J. Med. Chem. 49 (2006) 6596–6606, http://dx.doi.org/10.1021/jm0608210.

[112] B. Kuhn, P.A. Kollman, Binding of a diverse set of ligands to avidin and streptavidin: an accurate quantitative prediction of their relative affinities by a combination of molecular mechanics and continuum solvent models, J. Med. Chem. 43 (2000) 3786–3791, http://dx.doi.org/10.1021/jm000241h.

[113] C.H. Reynolds, M.K. Holloway, Thermodynamics of ligand binding and efficiency, ACS Med. Chem. Lett. 2 (2011) 433–437, http://dx.doi.org/10.1021/ml200010k.